RSC Advances

PAPER

View Article Online
View Journal | View Issue

Cite this: *RSC Adv.*, 2026, **16**, 17959

Pico-molar determination of lurasidone hydrochloride in pharmaceutical formulations using PVC-membrane bulk Miptode

Fatehy M. Abdel-Haleem,[a] Yomna M. Ahmed *[b] and Menna El-Beshlawy[c]

Lurasidone hydrochloride (LRH) is an important medication used for schizophrenia treatment, with minimal side effects of body weight loss, limited sedative capacity and minimal metabolic change; accordingly, its determination is vital, as it is recommended for psychological and memory problems. Molecularly imprinted (MIP) and non-imprinted polymers (NIP) were prepared, and their structures were confirmed by FTIR. MIP and NIP were used as ionophores in bulk membrane optodes (Miptode and Niptode) for LRH determination. Miptode incorporated MIP as an ionophore, tetraphenyl borate as an ion-exchanger, nitrophenyl octyl ether as a plasticizer, and ETH 2439 as a chromoionophore; the response mechanism involved host–guest MIP-LRH complexation *via* hydrogen bonding, as confirmed by FTIR, followed by deprotonation of the chromoionophore, which caused an absorbance decrease at 675 nm. Compared with Niptode and ion-exchanger-based optodes, Miptode exhibited a very wide concentration range of 10^{-11} to 10^{-4} M and a very low detection limit of 10 pM. The superior Miptode selectivity was confirmed by the separate solution and mixed solution methods; the mixed solution method exhibited changes in absorbance (% relative error) of 8, 33, and 29% for Miptode, Niptode, and the ion-exchanger-based optode, respectively. The wide linear concentration range, low detection limit, and high selectivity of Miptode were confirmed by the uniform particle size of the MIP at 47 nm and its homogeneous distribution, as observed by SEM and elemental mapping. Miptode was successfully applied to determine LRH in pure solutions, the pharmaceutical formulation Serodopamoun® tablets, and spiked urine samples, with reasonable accuracy (recovery: 98.5–102.3%) and high precision (relative standard deviation <0.81%). MIP is a suitable alternative for enhancing the ionophore library to prepare sensors for any analyte.

Received 11th October 2025
Accepted 10th March 2026

DOI: 10.1039/d5ra07784b

rsc.li/rsc-advances

1. Introduction

One strong antipsychotic medication is lurasidone hydrochloride (LRH), Fig. 1. It belongs to the benzisothiazol subsidiary synthetic class; its synthetic name is (3a*R*,4*S*,7*R*,7a*S*).2-{(1*R*,2*R*) and it is 2-[4-(1,2-benzisothiazyl) piperazin1ylmethyl] cyclohexylmethyl ∼ hexahydro-4,7-methano-2*H*-isoindole-1,3-dione hydrochloride.[1] LRH is marketed under the trade names Latuda® and Serodopamoun®; it is the preferred drug due to its minimal effects on body weight, limited sedative capacity, and lack of significant changes across metabolic limits.[1] For the treatment of schizophrenia and debilitating episodes associated with bipolar I disorder (bipolar wretchedness), LRH has FDA approval.[2,3] LRH may be able to help with the psychological and memory problems associated with schizophrenia.[3] Unlike other antipsychotics, it does not interfere with cholinergic effects, which are known to impair memory and mental cycles.[3] However, abnormal and irregular doses of LRH may cause severe problems such as cardiac and respiratory acute depression, which require fast intervention.[2] Also, prolonged use of LRH may cause a potentially reversible movement disorder; accordingly, several analytical methods have been reported for the determination of LRH.

LRH was determined using HPLC,[4,5] liquid chromatography,[1,6,7] and UV-visible spectrophotometry.[8] These methods are limited by the need for expensive, sophisticated instruments and by multiple sample preparation steps required before measurement,[9] which is particularly problematic in routine analysis or quality control. Electrochemical methods of analysis, such as voltammetry and potentiometry using an ion-selective electrode (ISE), offer the possibility of *in situ* measurement with a portable, simple electrode, which is well-suited for routine analysis.[10–12] In addition, other advantages, such as ease of measurement, the absence of sample preparatory steps, sensitivity to nanomolar concentrations, and a wide range of applications that extend to many orders of magnitude,

[a]*Department of Chemistry, College of Science, Imam Mohammad Ibn Saud Islamic University (IMSIU), Riyadh, 11623, Saudi Arabia. E-mail: FMMohamed@imamu.edu.sa*

[b]*Department of Chemistry, Faculty of Science, Cairo University, 12613 Giza, Egypt. E-mail: yomna@sci.cu.edu.eg*

[c]*Department of Chemistry, Faculty of Women, Ain Shams University, Cairo, Egypt. E-mail: Menna.El-Beshlawy@women.asu.edu.eg*

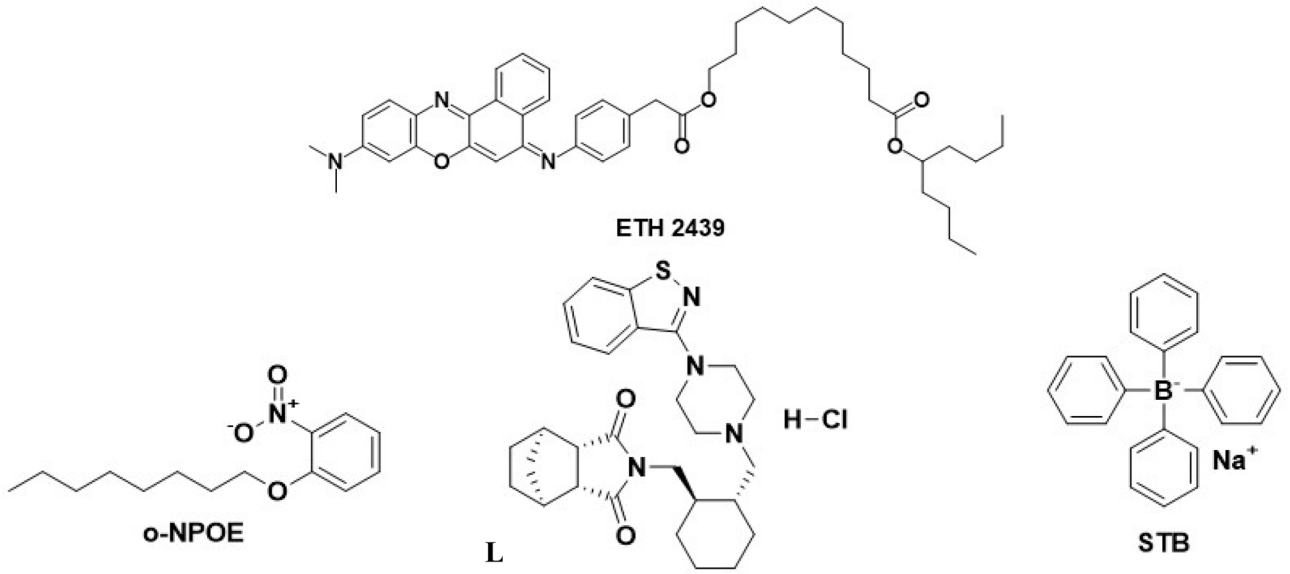

Fig. 1 Structure of the different components used in Miptode and Niptode fabrication.

are beneficial for analytical measurement purposes, making ISE a suitable candidate for the analysis of pharmaceutical species.[13] LRH was determined using a screen-printed electrode that is coated with polyaniline and a composite of polyvinyl-chloride (PVC)/Multi-Walled Carbon Nanotubes (MWCNTs)/ Molecularly-imprinted polymer (MIP).[3] Although the electrode's sensitivity extended to the nanomolar range, the sensor preparation involved several steps, including a polyaniline layer, followed by a PVC layer containing MWCNTs and MIP.[3]

One of the most effective analytical methods for determining various analytes is the use of bulk ion-selective optodes (ISOs).[11,14–16] Broad use of ISOs is due to a variety of interesting features, such as its low detection limit, pH cross-sensitivity that allows for variable linear dynamic range, ability to identify species with varying charges, lack of internal filling solution which facilitates miniaturization, quick reaction, inexpensive analysis, and no pretreatment procedures, simple and easy preparation, affordability, and suitability for routine analysis.[11,16–19] ISOs were used to determine cationic, anionic, and neutral species;[16,18] they were used in industrial, medical, and environmental applications.[16,17,20] These included enhanced analyte selectivity in a variety of matrices and other applications, with multiple improvements in substrate materials and sensing schemes.[18]

ISOs, also known as PVC membrane bulk optodes, are frequently composed of lipophilic materials; they include ionophores, indicator or chromoionophores, and ion exchangers.[18] The process relies on the indicator's protonated and deprotonated forms, which have different optical characteristics and allow the sensor to capture changes in protonation degree.[16,18] The precise tailoring of the chromoionophore molecule itself is the essential idea underlying H^+-chromoionophore-based optodes. As a result of this meticulous design, the molecule displays a reversible color change in response to a change in proton concentration, which is correlated with the concentration of analyte ions.[16,18] Similar to the properties of ISE, ISOs have the benefits of having a wide concentration range that can be controlled by adjusting solution pH and chromoionophore type, excellent and adjustable selectivity, and high sensitivity for toxic heavy metals that extends to ppb detection limit.[16,17,21] Using smartphones as detectors is an intriguing aspect of ISO that makes the detection process easier everywhere, on all scales.[18,22] Various membrane optode components, such as PVC polymer substrate, plasticizer, ion exchanger, and nanoparticle additions, can be tailored for response optimization.[18] The appropriate ionophore selection facilitates the optodes application for any analyte due to the great adaptability of the selective ionophores.[18,20]

Molecularly imprinted polymer (MIP) was used as a selective ionophore, as it is tailored in the presence of the analyte molecule, which is then removed from the polymer, forming a cavity that is suitable just for the analyte species in a key–lock relation; this makes these types of molecules of very high selectivity.[23,24] MIP particles were used as ionophores in ion-selective electrodes and were employed in various types of electrodes.[25–27] Although MIP ionophore-based optode (Miptode) is very limited due to solubility limitation of MIP particles within optode membrane cocktail, the selectivity is highly improved to considerable extent;[23,28] Miptode preparation, also facilitates the measurement of any analyte species (anionic, cationic, neutral), even if there is no specific ionophore, just by preparing MIP for this analyte.[23,28]

Our literature review indicates that there are no publications on the use of ISOs for LRH detection. On the other hand, reports have indicated limited sensitivity and selectivity, a short linear detection range, limited stability, and excessive response time for the methods reported for LRH determination. In the present work, these limitations are addressed by developing a highly selective bulk Miptode membrane based on MIP that responds to LRH with great discrimination against other interfering species present in pharmaceutical formulations. In addition,

the proposed method extends the linear concentration range, improves selectivity, reduces reaction time, and enables picomolar detection of LRH. The applicability of the developed Miptode is demonstrated by its use in determining LRH in the widely available and affordable Serodopamoun® tablets and spiked urine samples.

2. Experimental

2.1. Materials and solutions

LRH and its pharmaceutical formulation (Serodopamoun® 40 mg) were sourced from Amoun Pharmaceutical Co., S.A.E., Egypt; benzoyl peroxide (BPO, $C_{14}H_{10}O_4$, 95.0%), vinyl pyridine (VP, 98.5%), ethylene glycol dimethacrylate (EGDMA, 97.0%), chromoionophore ETH 2439)99.0%, Fig. 1), dimethyl sulfoxide (DMSO, 96.0%), sodium tetraphenyl borate (STB, 99.5%, Fig. 1), poly-vinyl chloride (PVC, high molecular weight, 98%), tetrahydrofuran (THF, 98.0%), dibutyl phthalate (DBP, 99%), and *o*-nitrophenyl octyl ether (NPOE, 99.0%, Fig. 1) were obtained from Sigma-Aldrich (Germany), and were used for the preparation of MIP-based and NIP-based optodes (Miptode and Niptode, respectively).

Hydrochloric acid (HCl, 30.0%), phosphoric acid (H_3PO_4, 97.0%), boric acid (H_3BO_3, 98.0%), sodium acetate ($C_2H_3NaO_2$, 98.0%), cobalt chloride ($CoCl_2$, 97%), sodium hydroxide (NaOH, 95.0%), acetic acid ($C_2H_4O_2$, 99.5%), silver nitrate ($AgNO_3$, 99.0%) and chloride salts of nickel ($NiCl_2$, 98%), sodium (NaCl, 99.0%), magnesium ($MgCl_2$, 98.5%), potassium (KCl, 99%), ammonium (NH_4Cl, 99.5%), and manganese ($MnCl_2$, 99%) were purchased from ADWIC, Cairo, Egypt, and were used for preparation of interfering ion solutions. Britton Robinson (BR) buffers of pH (7.4 and 3.0) were prepared using 0.04 M of each of boric acid, acetic acid and phosphoric acid, as described elsewhere.[29] Acetate buffer (pH 4.5) was prepared using acetic acid and sodium acetate. These buffers were used to prepare 10^{-2} M LRH, which was further diluted to prepare analyte solutions (10^{-3}–10^{-12} M), and the acetate buffer was used to prepare interfering-ion solutions.

2.2. Preparation of molecularly-imprinted (MIP) and non-imprinted polymers (NIP)

MIP and NIP of LRH were prepared and characterized using various techniques. For MIP preparation, a screw-capped Pyrex tube containing 20 mL of DMSO was filled with 3.0 mmol of the monomer (VP), 3 mmol of the cross-linker (EGDMA), and 1.0 mmol of the template (LRH); 60.0 mg of the initiator (BPO) was gradually added, and the mixture was degassed with a stream of pure Argon for five minutes before being placed in an oil bath at 60 °C for 24 hours; a white solid was produced, which was finely ground with a mortar and a pestle before being sieved to a size of ~45 μm.[3] The polymer's particles were dispersed in a 9 : 1 v/v methanol-acetic acid mixture for a day, and then filtered and reconstituted in methanol and deionized water for another day in order to extract LRH. Using spectrophotometry, the LRH elimination was confirmed at 263 nm. Without the addition of LRH, NIP was methodically prepared using the same procedure.[3]

2.3. Equilibrium binding assay

To determine the binding properties of polymers, 20 mg of the prepared MIP or NIP particles were added to 1 mL of different concentrations of LRH prepared in a 1 mL Eppendorf tube and then shaken for 2 h at room temperature. The solution was then centrifuged (10 min. at 10 000 rpm), and the resulting supernatant was further filtered using a 0.22 μm syringe filter. The concentration of remaining LRH in the supernatant was determined at 263 nm by spectrophotometric measurements.

The binding capacities (B, mmol g^{-1}) for MIP and NIP are calculated by eqn (1):[30]

$$B = \frac{(C_i - C_f)V}{M} \quad (1)$$

where C_i and C_f are the initial LRH concentration and the concentration after adsorption (mM), respectively, V is the volume (mL), and M is the polymer particles mass (g). The imprinting factor (IF) was calculated by the binding capacity of the imprinted polymer to that of the non-imprinted one, according to eqn (2):[30,31]

$$\mathrm{IF} = \frac{B(\mathrm{MIP})}{B(\mathrm{NIP})} \quad (2)$$

To determine the binding isotherms and to perform Scatchard analysis for MIP, 20 mg of the MIP was incubated with 1 mL of LRH (1.0×10^{-8}–1.0×10^{-6}M) prepared in water.

The binding isotherm of LRH to the MIP and NIP was studied in terms of the Langmuir and the Freundlich isotherms according to eqn (3) and (4):[32–35]

$$\frac{1}{B} = \frac{1}{K_L B_{max}} \times \frac{1}{C_e} + \frac{1}{B_{max}} \quad (3)$$

$$\log B = \log K_F + \frac{1}{n} \log C_e \quad (4)$$

where B is the binding capacity of the polymer in nmol g^{-1}, C_e is the final free LRH concentration at equilibrium in nM, B_{max} is the maximum binding capacity in nmol g^{-1}, K_L and K_F are the Langmuir and Freundlich constants, respectively, and finally n is the adsorption intensity in L g^{-1}.

2.4. Manufacturing of Miptode, Niptode and ion-exchanger-based optode

In the presence of the chromionophore ETH2439 and the ion exchanger STB, the membrane optodes created in this work offer an alternative for tracking LRH levels. Optode spectra were measured and recorded using a UV-vis spectrophotometer (UV-vis OPTIZEN POP, Korea). pH measurements were performed using a pH meter (Adwa AD1030, Hungary). Various types and quantities of optode components were used to optimize the composition of the Miptode and Niptode; the amounts of PVC, ETH 2439 chromoionophore, plasticizer, the ionophore (MIP or NIP) and ion-exchanger were changed for preparation of Miptode or Niptode, respectively; an ion-exchanger-based optode was prepared using the same components without addition of the ionophore. The different membrane components were

dissolved in 2 mL THF until forming homogenous cocktail, which was casted onto a dust-free quartz slide (0.9 × 4 cm^2, 1 mm thick). The cocktail on the quartz slide was allowed to dry in the air for roughly 10 minutes to form an optode, and it was kept in the dark when not in use.

2.5. Spectral measurements

The absorbance of Miptode, Niptode or IE-based optode was measured in a quartz cuvette (1 × 1 × 4 cm^3) containing the analyte and/or interfering solution. The spectra of the several optodes were captured, and the calibration curves were constructed at the specific maximum wavelength (λ_{max}) of 675 nm of ETH 2439.[36] Before the initial measurement, the Miptode and Niptode were conditioned in buffer for 20 min. The spectra of a chromoionophore-free optode were recorded for background correction. The absorbances of the different optodes were measured for the fully deprotonated (A_1) and fully protonated (A_0) forms of the chromoionophores in 0.1 M NaOH and 0.1 M HCl, respectively.[14] For the calculation of the normalized absorbance (α values), which is the fraction of the total optode membrane chromoionophore ($[C_m^T]$) that is present in the deprotonated form ($[C_m^-]$), α can be expressed in terms of measurable quantities in eqn (5):[14]

$$\alpha = \frac{A - A_0}{A_1 - A_0} = \frac{[C_m^-]}{[C_m^T]} \quad (5)$$

2.6. Effect of pH

Optode measurement is characterized by the change of linear dynamic range as the solution pH changes, due to the presence of a pH-dependent chromoionophore, which is termed pH cross-sensitivity.[16] BR buffer (pH 7.4 and 3.0) and acetate buffer (pH 4.5) were prepared and tested throughout the work. The buffer exhibiting the best response characteristics was selected.

2.7. Selectivity

The Miptode and Niptode selectivity were assessed using the separate solution method and mixed solution method.[15,16,37] In separate solution method, the absorbance of the different concentrations of analyte and interfering ions (10^{-8}–10^{-6} M) is measured at 675 nm, and calibration curves are plotted for analyte and interfering ions; selectivity coefficients are calculated from the figure at $\alpha = 0.5$.[16] In mixed solution method, different amounts of 10^{-2} M of the interferent solutions were added to 10^{-4} M LRH solution, and the absorbance shift was recorded to calculate the relative error. Common cations (Na^+, K^+, Mg^{2+}, Ni^{2+}, Pb^{2+}, Ag^+, Mn^{2+}, NH_4^+, and Co^{2+}) that may coexist with analyte ion in pharmaceutical formulation or biological samples, were selected. The selectivity measurement was performed for Miptode, Niptode and ion-exchanger-based optode.

2.8. Response time and lifetime

The stability of the Miptode signal was recorded at various times; *i.e.*, the time required to achieve about 90% of the stable signal was recorded and considered the response time.[11] To obtain the lifetime, calibration curve measurements were performed using Miptode at different time intervals, and the changes in linear dynamic range and detection limit were recorded.

2.9. Determination of LRH in tablets and spiked urine samples

The optimized Miptode was used to determine unknown pure LRH solutions, solutions of the pharmaceutical preparation Serodopamoun®, and spiked urine samples using the direct calibration method. For pharmaceutical formulation analysis, five Serodopamoun® tablets were ground as fine powder, precisely weighed, dissolved in acetate buffer, and filtered through a syringe filter, and used for the preparation of 10^{-4} M LRH solution using acetate buffer; the appropriate dilutions were prepared as 10^{-5} and 10^{-6} M LRH solutions. (10^{-8} to 10^{-6} M) spiked urine samples were prepared by spiking 2.0 mL urine of healthy person (corresponding author) with different volumes of 10^{-4} M LRH solution and completing to exact volume using acetate buffer. The constructed Miptode was used to determine LRH in these solutions, and recovery was calculated. Statistical calculations are performed to confirm the accuracy and precision of the Miptode, where each sample was measured three times.

3. Result and discussion

3.1. Equilibrium rebinding and adsorption isotherm analysis

The binding performance of MIP and NIP was evaluated using batch rebinding experiments using an LRH concentration range of (10^{-8}–10^{-6} M). Equilibrium concentrations were calculated after interaction with MIP or NIP by absorbance measurement. From the obtained results, it was found that MIP exhibited an imprinting factor (IF) of 3.5, indicating enhanced binding of LRH to the MIP, and that the adsorption of LRH to the MIP is not solely due to nonspecific interactions, but also due to the presence of binding cavities compatible with the size and functional groups of LRH.

Furthermore, the adsorption isotherms of both MIP and NIP were evaluated using the Langmuir and the Freundlich isotherms; the results are shown in Fig. 2 and listed in Table 1. The MIP adsorption isotherm follows both models, with a superior fit to the Langmuir model, as indicated by the R^2 value (0.9998). This means that the adsorption of LRH is assumed to follow a monolayer adsorption on a homogeneous surface. On the other hand, the NIP adsorption isotherm more closely follows the Freundlich isotherm as also evident in the R^2 value (0.9998).[32–35]

Moreover, the maximum adsorption capacities (B_{max}) for chemisorption and physisorption were calculated for LRH adsorption on MIP and NIP from the Langmuir isotherm model, indicating that the B_{max} of 57.06 and 4.29 nmol g^{-1} for LRH adsorption onto MIP and NIP, respectively, demonstrating the effectiveness of MIP in binding LRH from solution. In addition, the Langmuir constant (K_L) was larger for MIP than for NIP, reflecting stronger interaction between LRH and the imprinted sites in MIP.[32–35]

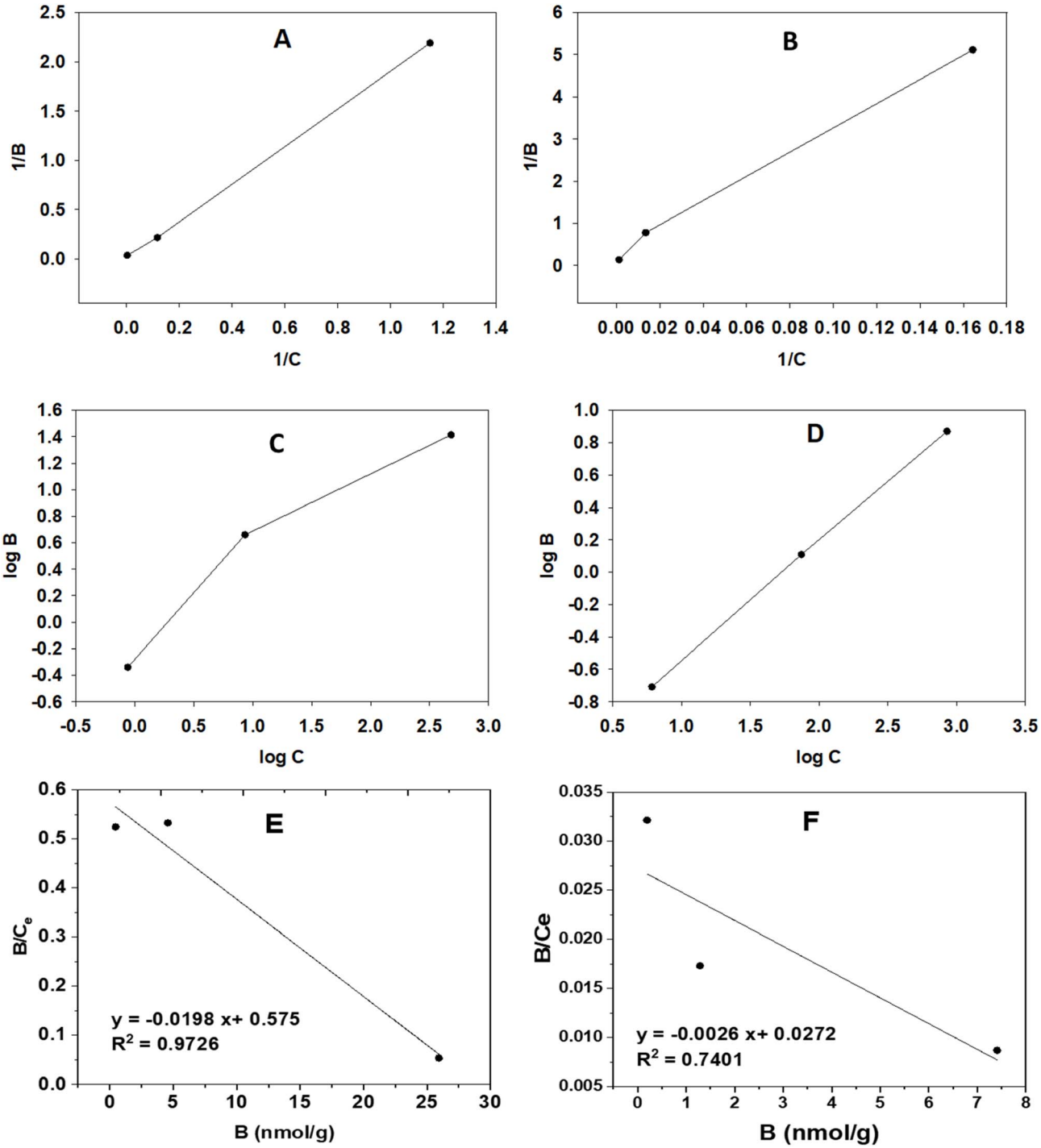

Fig. 2 Langmuir adsorption isotherm curves for MIP (A) and NIP (B). Freundlich isotherm curves for MIP (C) and NIP (D). Scatchard analysis for MIP (E) and NIP (F).

In contrast, the Freundlich isotherm evaluates surface heterogeneity and adsorption intensity (n). As shown in Table 1, n for MIP was greater than unity, and greater than that for NIP, thus indicating a high distribution of binding sites.[32–35] Moreover, the Freundlich constant (K_F) for MIP was higher than that for NIP.

The Scatchard model was used to characterize the affinity distribution of MIP's binding sites using eqn (6):

$$\frac{B}{C_e} = K_a B_{max} - K_a C_a \quad (6)$$

where B is the binding capacity of the MIP in nmol g^{-1}, C_e is the LRH equilibrium concentration in nM, B_{max} is the apparent maximum binding capacity, and K_a is the association constant in nM^{-1}, respectively. As shown in Fig. 2E, MIP showed a linear Scatchard plot ($R^2 = 0.973$) with a negative slope consistent with adsorption behavior. In contrast, NIP (Fig. 2F) showed poor

Table 1 MIP and NIP isotherm parameters for LRH binding

Model	Parameter	Unit	MIP	NIP
Langmuir	B_{max}	nmol g^{-1}	57.06	4.29
	K_L	L g^{-1}	0.0093	0.0078
	R^2		**0.9998**	0.9974
Freundlich	n	g L^{-1}	1.624	1.360
	K_F	nmol g^{-1}	0.168	0.020
	R^2		0.9440	**0.9998**
Scatchard	B_{max}	nmol g^{-1}	29.044	10.347
	K_a	nM^{-1}	0.0198	0.0026
	K_d[a]	nM	50.513	381.00

[a] K_d: dissociation constant (the reciprocal of association constant).

linearity (R^2 = 0.770) with a smaller slope, proving a weaker interaction with LRH. As shown in Table 1, the MIP exhibited a maximum apparent binding capacity of 29.044 nmol g^{-1} with an association constant of 0.0198 nM^{-1}, higher than those obtained for NIP, indicating stronger LRH-MIP binding.

3.2. Chemical bonding and morphology of MIP and NIP nanoparticles

The synthesis of MIP and NIP involved meticulous control over polymerization conditions to achieve specific molecular recognition capabilities. In the case of MIP, the process began with the mixture of VP monomers and EGDMA crosslinker in acetonitrile solvent. BPO acts as the initiator, generating free radicals at elevated temperatures to initiate polymerization. The template molecule, LRH, interacted with VP monomers *via* noncovalent interactions, including hydrogen bonding and van der Waals forces. This interaction guided the formation of selective binding sites within the polymer matrix that mimic LRH's size, shape, and functional groups. Concurrently, EGDMA crosslinked the polymer chains, forming a 3D network that stabilizes the imprinted cavities. Post-polymerization, the removal of LRH from the polymer matrix was crucial to unveil the imprinted sites. Extraction with acetic acid and methanol mixture solution removed the template molecule, leaving behind specific binding sites that retain molecular recognition characteristics. This step ensured that MIP retains high selectivity and affinity towards LRH even after template removal. In contrast, NIP was synthesized under identical conditions but without LRH, resulting in polymers with randomly distributed binding sites and with no selectivity. The absence of the template molecule in NIP led to a lack of specific molecular recognition, highlighting the critical role of molecular imprinting in enhancing the polymer's selectivity and sensitivity for the targeted analyte, LRH.

FTIR analysis was employed to provide molecular-level evidence of LUR binding within the polymeric matrix, as recommended by G. D. Middeleer *et al.*[38] The FTIR spectra of MIP, unwashed MIP (MIP-LRH complex) and NIP are presented in Fig. 3. Clear spectral differences between these materials provide evidence for successful imprinting and drug–polymer interactions. The spectra of MIP and MIP-LRH confirmed the hydrogen–bonding interaction between MIP and LUR, as evident in the broad band assigned to both N–H and O–H at about 3400 cm^{-1} in the MIP-LRH complex is absent in MIP and NIP spectra, confirming the success of the imprinting process. Also, the C–Cl band is very weak in the case of MIP and NIP, so the washing process for LRH removal to form MIP was good.[2,39,40] Bands of MIP at 1690, 2932, 1138, and 742 cm^{-1} assigned to ketone C=O, aromatic C–H, C–N of the amine, and C–Cl are shifted to 1684, 2950, 1150 and 712 cm^{-1} after interaction with LRH (MIP-LRH in the unwashed MIP), respectively, Fig. 3.[2,39,40] The key bands of LRH assigned to N–H or O–H, aromatic C–H and C–Cl are completely absent or very weak in the case of NIP spectra, where the peak of aryl C=O existed at different positions for MIP (1684 cm^{-1}) and NIP (1726 cm^{-1}), which can be assigned to the keto group of monomers; these

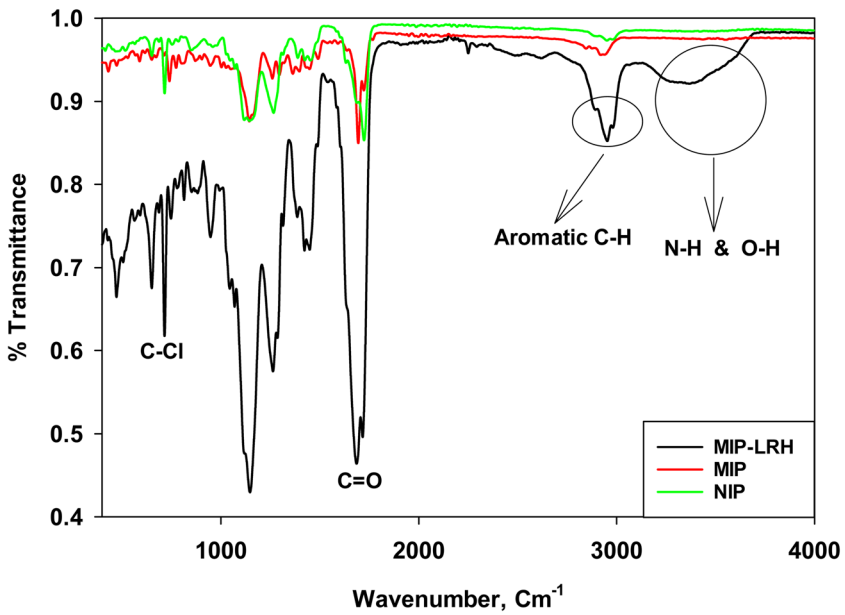

Fig. 3 FTIR of MIP particles before (red) and after interaction with LRH (black), and NIP particles (green).

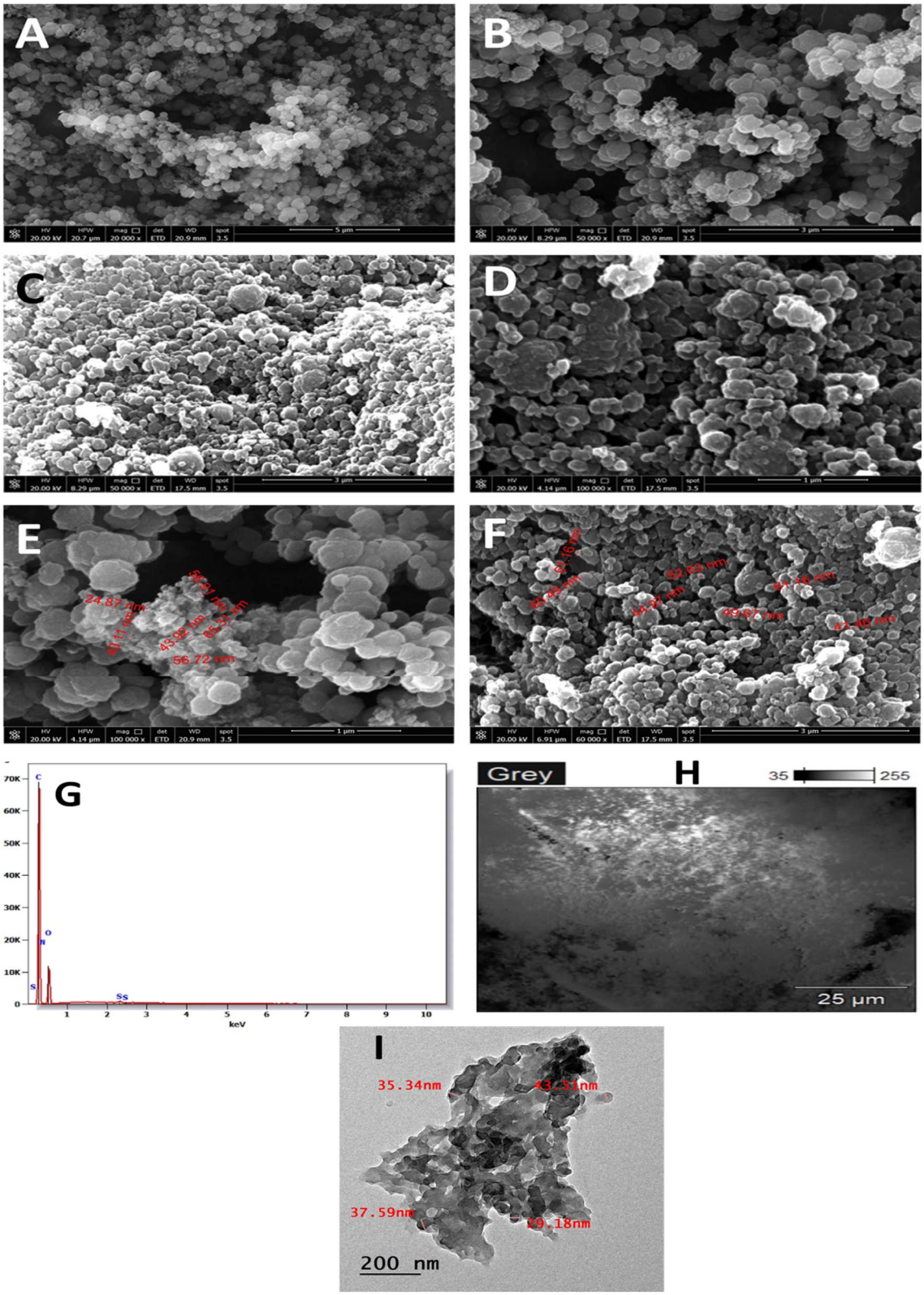

Fig. 4 SEM analysis and elemental mapping: SEM images reveal the morphologies and particle size distributions of MIP and NIP, with (A, B and E) showing the uniform spherical morphology of MIP of average particle sizes of 47 nm with scale bar and (C, D and F) displaying the NIP particles of size 40 nm and its agglomerates of 250 nm sizes with scale bar. (G and H) SEM-EDS elemental mapping of MIP illustrates the presence and distribution of carbon. (I) TEM of MIP particles.

confirm the success of imprinting process. Collectively, these spectral observations provide strong evidence for successful template incorporation, specific binding interactions, and the formation of well-defined imprinted cavities within the MIP.

The structure and morphology of MIP and NIP were studied by imaging their particles using SEM and TEM. As shown in Fig. 4, MIP and NIP particles appear spherical and semi-uniform, with average diameters range of 30–60 nm, ensuring a similar particle distribution across the membrane optode. However, Fig. 4 shows NIP particles are randomly agglomerated and coagulated. The MIP's particles are more organized, due to structured polymerization process using LRH, which interacts with the VP monomer and the EGDMA crosslinker *via* host–guest hydrogen bonding, thereby forming selective binding sites.[41] However, LRH is absent in NIP cases, leading to random polymerization, a less structured network, and irregular particles.[42] The elemental mapping of the MIP in Fig. 4 shows the homogenous presence of carbon.

3.3. Effect of composition and response mechanism

The membrane composition determines the optode's sensitivity and selectivity. To optimize Miptode performance, its composition was varied by changing the types of ionophore; the type of plasticizer, the amount of ion-exchanger, the amounts of (PVC, plasticizer, and ETH 2439) were fixed, Table 2. The existence of an ion-exchanger is mandatory for sensors that operate by a neutral carrier mechanism.[16] The influence of these variables was carefully assessed to improve the Miptode overall detection capabilities.

The comparison between Miptode 1 and Niptode 2 highlights the significant impact of using MIP and NIP as the ionophore. Both optodes contained the same plasticizer (NPOE), ion-exchanger (TPB), and ionophore concentration (0.0060 g). However, Miptode 1 exhibited sigmoidal and shape better response characteristics, including a very broad linear dynamic range (10^{-11}–10^{-4} M), a higher linear absorbance change per concentration (lower curve in Fig. 5), and the lowest detection limit (1.0×10^{-11} M). These results indicate that MIP significantly enhances sensitivity and selectivity by providing tailored binding sites for LRH, confirming host–guest complexation. Although Niptode exhibited good response for LRH, the absorbance change is not linear and there are two concentration ranges (10^{-11}–10^{-10} and 10^{-7}–10^{-4} M); it can be accounted for the Niptode response by the non-selective hydrogen bonding interaction that takes place on the surface of NIP particles, but the NIP lacks such specificity, due to the absence of selective cavities, as will be shown in selectivity part.[3]

For comparison, IE-optode 3 was prepared without an ionophore to confirm the role of MIP in LRH recognition. This IE-optode 3 displayed analytical response to LRH in a narrower linear dynamic range (10^{-11}–10^{-6} M); this response is mainly due to the ion-exchange process, but the absence of MIP particles causes deterioration in the concentration range, the sensitivity and selectivity, confirming that the MIP plays a crucial role in the optode's response.

Additionally, the plasticizer affects the mobility of the optode components, thereby strongly influencing the optode response. Therefore, two different plasticizers were examined: *o*-NPOE and DBP. Miptode 4 incorporated DBP while maintaining the same other component amounts as those of Miptode 1. However, its performance data (linear dynamic range, absorbance difference between highest and lowest concentrations = ΔA, and detection limit) were not recorded, indicating that DBP was unsuitable for this study.

Fig. 5 shows the spectrum of Miptode 1 for LRH concentrations ranging from 10^{-11} to 10^{-4} M in acetate buffer (pH 4.5), with a maximum at 675 nm. The detection limit was determined according to method reported by Bakker *et al.*; when there is a sigmoidal response that results in loss of response, the detection limit is defined as the concentration at which sensitivity is lost and response slope decreases to one-half of the maximum slope.[16] In conclusion, among the tested compositions, Miptode 1 exhibited the most favorable analytical characteristics, indicating that the combination of MIP as the ionophore, *o*-NPOE as the plasticizer, and TPB as the ion-exchanger is optimal for enhancing the Miptode response. Thus, Miptode 1 was chosen for carrying out further experiments.

The Miptode response mechanism can be elucidated from previous results in eqn (7):[43]

$$CH_m^+ + MIP_m + LRH_a^+ + R_m^- \leftrightarrow C_m + H_a^+ + MIP\text{-}LRH_m^+ + R_m^- \quad (7)$$

where CH_m^+ and C_m represent the protonated and deprotonated chromoionophore (ETH 2439) in the membrane phase, respectively; MIP_m and $MIP\text{-}LRH_m^+$ are the free and complexed MIP in the membrane phase; LRH_a^+ and H_a^+ are the LRH and proton in the aqueous phase, respectively; R_m^- is the lipophilic

Table 2 Composition of different Miptodes, Niptode and ion exchanger-based optode with linear dynamic range and detection limits[a]

	Composition, g						
No.	PVC	Plasticizer	ETH 2439	Ionophore	TPB	Linear dynamic range, M	Detection limit, pM
Miptode 1	0.030	0.060 N	0.001	0.0060 MIP	0.002	10^{-11}–10^{-4}	10.0 ± 0.07
Niptode 2	0.030	0.060 N	0.001	0.0060 NIP	0.002	10^{-11}–10^{-10} and 10^{-7}–10^{-4}	10.0 ± 0.09
IE-optode 3	0.030	0.060 N	0.001	—	0.002	10^{-11}–10^{-6}	10.0 ± 0.03
Miptode 4	0.030	0.060 D	0.001	0.0060 MIP	0.002	—	—

[a] IE-optode: ion-exchanger based optode, N: *o*-NPOE, D: DBP, pM: pico-Molar.

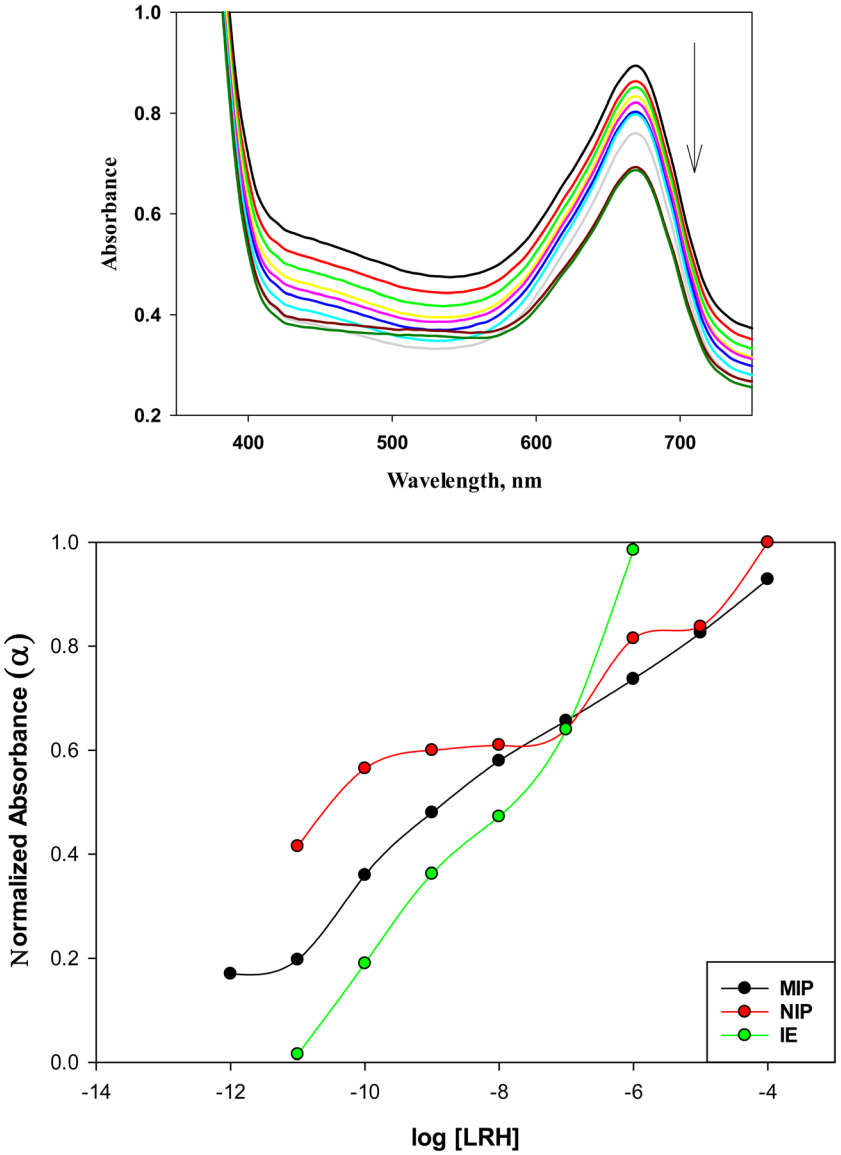

Fig. 5 (UPPER)Spectrum of Miptode 1 in the concentration range of 10^{-11}–10^{-4} M LRH in acetate buffer pH 4.5, maximum at 675 nm; (LOWER) calibration curves of Miptode, Niptode and IE-optode.

anionic additive (TPB^-) that is used to maintain electroneutrality within the membrane.

As represented in Fig. 6, the optode membrane interfaces with the sample solution, allowing the analyte ions (LRH^+) to passively distribute between the aqueous phase and the organic sensing membrane phase until thermodynamic equilibrium is achieved.[43] The plasticizer and PVC matrix facilitate LRH^+ partitioning within the membrane, thereby increasing the

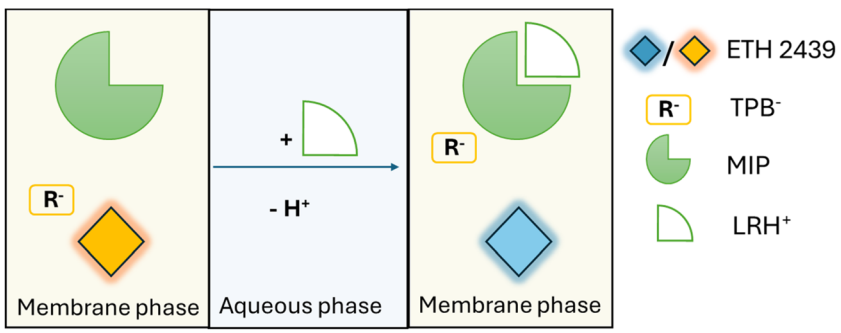

Fig. 6 Schematic illustration of the response mechanism of Miptode 1.

Table 3 Analytical performance of Miptode 1 at different pH values in acetate and BR buffers

pH- buffer	C.R., M	D.L., M
3.0 – BR	—	—
4.5 – acetate	10^{-11}–10^{-4}	1.0×10^{-11}
7.4 – BR	10^{-10}–10^{-7}	1.0×10^{-11}

probability of encountering the MIP sites. Once incorporated into the membrane, the LRH^+ ions form a stable complex with the neutral MIP ionophore, which contains cavities and chemical functionalities that selectively bind LRH^+ *via* host–guest interactions. As a consequence of the extraction of the LRH^+ cations, the chromoionophore concomitantly loses a proton to re-establish the membrane's electroneutrality, triggering an optical response with a decrease in absorbance at 675 nm. The magnitude of absorbance change is proportional to the extent of ion extraction and, therefore, the analyte (LRH^+) concentration. The high MIP recognition narrows which ions partition into the membrane, reducing background noise and therefore enabling the exceptionally low detection limit.[44]

3.4. pH effect

In optodes, signal transduction occurs through the chromoionophore, which relies on its protonation–deprotonation equilibrium to generate an optical response.[16] A key advantage of this pH-dependent cross-response is the ability to adjust the sensor's linear dynamic range.[11] Miptode 1 performance was tested at pHs 3.0, 4.5, and 7.4, see Table 3. The best performance was obtained in acetate buffer at pH 4.5, with the widest linear dynamic range of 10^{-11}–10^{-4} M. at pH 3.0; direct chromoionphore protonation by buffer may account for diminished response; the diminished response at high pH of 7.4 can be accounted for by the lower amount of LRH that exists in the cationic form, where pK_a of LRH is 8.5. Accordingly, pH 4.5 was selected for further measurements.

3.5. Selectivity

The separation solutions method was performed to testify the selectivity of the Miptode 1 in the presence of various monovalent (Na^+, K^+, NH_4^+, and Ag^+) and divalent ions (Mg^{2+}, Mn^{2+}, Co^{2+}, Ni^{2+} and Pb^{2+}); it was found that ions that can form hydrogen bonding with MIP (NH_4^+), and ions of large size (Ni^{2+} and Pb^{2+}) which can do host–guest interaction within membrane cavity, exhibits slight interference, Table 1. However, separation solutions method is not a measure for the real application, where the analyte and interfering solutions are measured separately.[16] The mixed solution method[45] was used to evaluate the selectivity of the optodes for LRH in presence of the mentioned interfering ions. To highlight the influence of composition on the sensor's selectivity behavior, Miptode 1, Niptode 2, and IE-optode 3 were tested. The absorbance signals of the studied optodes were recorded in the presence (A) and absence (A_0) of interfering ions, and the relative error (% R.E.) was calculated according to eqn (8):[45]

$$\%\ \text{R.E.} = [(A - A_0)/A_0] \times 100 \quad (8)$$

As shown in Table 4, Miptode 1 exhibited better selectivity behavior than other optodes, as evident in the lower % R.E. values. The results provide insight into the role of MIP in stabilizing LRH target ions within the organic optode membrane phase, thereby enhancing sensor selectivity and minimizing interference from competing ions. Results of

Table 5 Determination of LRH in pure solutions, pharmaceutical formulation (Serodopamoun® tablets), and spiked urine sample

Taken, M	Recovery%	RSD% ($n = 3$)
Pure solutions		
10^{-6}	98.5	0.72
10^{-5}	102.3	0.61
Serodopamoun®		
10^{-6}	99.4	0.47
10^{-5}	101.1	0.81
Spiked urine		
10^{-8}	91.2	1.1
10^{-7}	97.0	0.4
10^{-6}	96.3	0.3

Table 4 Selectivity test by separate and mixed solutions methods

	Log K separate solutions method	R.E. % (mixed solutions method)		
Species	Miptode 1	Miptode 1	Niptode 2	IE-optode 3
Na^+	−1.5	1.305	3.191	6.441
K^+	−3.5	−0.522	3.723	11.864
NH_4^+	>1	5.714	30.070	12.203
Ag^+	−1.0	4.439	16.783	25.763
Mg^{2+}	−2.5	6.915	27.208	15.254
Mn^{2+}	<−6.0	−1.064	14.841	18.305
Co^{2+}	−1.0	1.8288	33.922	3.051
Ni^{2+}	>1	7.979	20.141	−29.153
Pb^{2+}	>1	6.383	22.968	−10.169

Table 6 Comparison of the analytical performance of the proposed PVC membrane bulk Miptode with previously reported methods for LRH determination[a]

	This work	47	3	5
Method/Sensor	**Miptode**	PET	PVC/MIP/MWCNTs/PANI/SPE	RP-HPLC
Concentration range	**10^{-11}–10^{-4}M**	30 – 1600 ng mL^{-1}	10^{-8}–10^{-4} M	4.7×10^{-5}–2.8×10^{-4} M
Detection limit	**1.0×10^{-11}M**	12.9 ng mL^{-1}	1.0×10^{-8} M	1.3×10^{-7} M
Response time	**1–2 min**	—	2–3 min	—
Lifetime	**10 days**	—	15 days	—

[a] Miptode: molecularly-imprinted polymer-based bulk membrane optode, PET: photo-induced electron transfer, PVC/MIP/MWCNTs/PANI/SPE: PVC/imprinted polymer/multi-walled carbon nanotubes layer deposited onto polyaniline-coated screen-printed electrodes, RP-HPLC: reversed phase high performance liquid chromatography.

Miptode 1 by separate solutions method nearly matches that of mixed solutions method. In the case of Niptode 2, the lower selectivity is due to the lack of Key–lock interaction between the NIP and LRH. In the absence of an ionophore in the case of IE-optode 3, the optode exhibits the highest R.E.% values, indicating that the ion-exchanger alone is not sufficient for the determination of LRH, where the response depends only on the ion-exchange process, which is controlled by thermodynamics only.

3.6. Response time and lifetime

The response time (T_R) is the time the sensor takes to reach 90% of its stable response.[16] According to Bakker *et al.*,[11] the response time of ISO is governed by the diffusion of all mobile species through the sensing organic membrane and the aqueous sample phase. The T_R for Miptode 1 was 1–2 min. The Miptode could be used successfully for measurements through a period of 10 days with minimum deviation in its response characteristics. This relatively limited stability can be due to the gradual leaching of membrane components, particularly the plasticizer and loosely embedded MIP particles, into the aqueous phase. In addition, prolonged exposure to the sample solution may lead to partial saturation or fouling of the imprinted binding sites, further contributing to signal deterioration over time. Moreover, optodes employing ETH 2439 have reported dye loss into the solution during conditioning.[46] Furthermore, E. Bakker *et al.* indicated that exposure of ETH 2439 to light and humidity can cause a decrease in response of around 8% within 10 h.[44] Such factors can alter the membrane microenvironment, affecting analyte partitioning and signal transduction.

Although the incorporation of MIP particles enhances selectivity, it may also introduce structural heterogeneity within the membrane, which can slightly increase response time and influence long-term stability. These factors collectively account for the observed response characteristics and define the current limitations of the developed sensor.

3.7 Application

Showing the widest linear dynamic range, the lowest detection limit, and the highest selectivity, Miptode 1 was used to determine LRH in pure solutions, a pharmaceutical formulation (Serodopamoun® tablets) at two concentrations, 10^{-6} and 10^{-5} M, and in spiked urine samples, using a direct calibration method. The findings in Table 5 revealed that the recovery% values ranged from 91.2% to 102.3%, which lie within the accepted threshold, confirming the reliability of the sensor. Moreover, the sensor showed high precision, as evidenced by the low RSD% values.

In comparison to previous recent works, Table 6, Miptode is characterized by its ease of preparation, fast response time, wide dynamic range, and lower detection limit.

4. Conclusion

Molecularly-imprinted polymer (MIP)-based bulk membrane optode (Miptode) was prepared and used for the determination of lurasidone hydrochloride (LRH) in its pure form, the pharmaceutical formulation Serodopamoun®, and in spiked urine samples. The preparation of MIP resulted in particles of nano-size (30–60 nm), which facilitate optimal characteristics of the miptode, including a wide linear concentration range and a low detection limit. In comparison to Niptode and ion-exchanger-based optode, Miptode exhibited superior selectivity due to the presence of cavities suitable for the LRH analyte; LRH interacts with MIP *via* host–guest (key–lock) hydrogen-bonding complexation. Miptode was successfully applied to LRH determination in real samples, with high accuracy and precision. A Miptode can be tailored for any type of analytes. To increase Miptodes' lifetimes, the designed optodes are recommended to be stored in the dark when not in use, especially those made using the Nile blue derivative chromoionophore ETH 2439. Moreover, research often focuses on improving the lipophilicity of the dyes or using plasticizer-free membranes.

Conflicts of interest

The authors have no conflict to declare.

Data availability

All data supporting the results are available as part of the article, and no additional data is available.

Supplementary information (SI) is available. See DOI: https://doi.org/10.1039/d5ra07784b.

Acknowledgements

This work was supported and funded by the Deanship of Scientific Research at Imam Mohammad Ibn Saud Islamic University (IMSIU) (grant number IMSIU-DDRSP2603).

References

1 M. Y. Katteboina, N. R. Pilli, R. Mullangi, R. R. Seelam and S. R. Satla, LC-MS/MS assay for the determination of lurasidone and its active metabolite, ID-14283 in human plasma and its application to a clinical pharmacokinetic study, *Biomed. Chromatogr.*, 2016, **30**, 1065–1074, DOI: 10.1002/BMC.3651.

2 J. R. Madan, K. T. Pawar and K. Dua, Solubility enhancement studies on lurasidone hydrochloride using mixed hydrotropy, *Int. J. Pharm. Investig.*, 2015, **5**, 114, DOI: 10.4103/2230-973X.153390.

3 M. M. El-Beshlawy, A. Barhoum and F. M. Abdel-Haleem, Nanomolar detection of lurasidone hydrochloride in pharmaceutical formulations (Serodopamoun®) and spiked urine using a PVC/imprinted polymer/MWCNTs layer deposited onto polyaniline-coated screen-printed electrodes, *RSC Adv.*, 2024, **14**, 39769–39778, DOI: 10.1039/D4RA07098D.

4 C. Liu, Q. Li, J. Fan, X. Bai, M. Wang and Y. Rong, *Determination of Lurasidone Hydrochloride Tablets by HPLC, China Pharmacist*, 2014, pp. 1483–1485, accessed December 29, 2024.

5 B. A. Ramprasad, S. Chaurasia and I. Singh, Advanced stability-indicating RP-HPLC method for the quantification of lurasidone hydrochloride in bulk and PLGA-based in situ implant formulation, *Ann. Pharm. Fr.*, 2025, **83**, 342–357, DOI: 10.1016/j.pharma.2024.10.008.

6 O. Siddig, C. Liu, M. Abdulbagi, M. Song, Y. ting Lu and T. jun Hang, Separation and characterization of related substances of Lurasidone hydrochloride by LC-QTOF-MS techniques, *J. Pharm. Biomed. Anal.*, 2024, **238**, 115834, DOI: 10.1016/J.JPBA.2023.115834.

7 S. Jia and Q. Liu, Method for Separating and Measuring Lurasidone Hydrochloride Intermediate Related Substances through Liquid Chromatography, *China Pat.*, CN105891392A, Beijing Venturepharm Biotech Co., Ltd., 2016, available at: https://patents.google.com/patent/CN105891392A/en.

8 K. V. Sri, S. Sravani and M. S. Kumar, Development and Validation of UV Spectrophotometric Method for Estimation of Lurasidone in Bulk and Pharmaceutical Formulations, *Asian J. Pharmaceut. Res.*, 2015, **5**, 102–107, DOI: 10.5958/2231-5691.2015.00015.5.

9 P. R. Satti, B. Vallamkonda and S. Sharma, Vinod, Quantitative analysis of nitrosamine impurities using liquid chromatography tandem mass spectrometry, *Pure Appl. Chem.*, 2026, **98**(3), 443–473, DOI: 10.1515/pac-2024-0397.

10 J. Wu, X. Yue, T. Wang, Y. Zhang, Y. Jin and G. Li, A cost-effective and sensitive voltammetric sensor for determination of baicalein in herbal medicine based on shuttle-shape α-Fe2O3 nanoparticle decorated multi-walled carbon nanotubes, *Colloids Surf., A*, 2025, **717**, 136850, DOI: 10.1016/j.colsurfa.2025.136850.

11 X. Xie and E. Bakker, Ion Selective Optodes: from the Bulk to the Nanoscale, *Anal. Bioanal. Chem*, 2015, **407**, DOI: 10.1007/s00216-014-8413-4.

12 E. Bakker and E. Pretsch, Potentiometric sensors for trace-level analysis, *TrAC, Trends Anal. Chem.*, 2005, **24**, DOI: 10.1016/j.trac.2005.01.003.

13 N. Jadon, B. Hosseinzadeh, S. I. Kaya, G. Ozcelikay-Akyildiz, A. Cetinkaya and S. A. Ozkan, Emerging trends of ion-selective electrodes in pharmaceutical applications, *Electrochim. Acta*, 2024, **488**, 144204, DOI: 10.1016/J.ELECTACTA.2024.144204.

14 F. M. Abdel-Haleem and R. M. El Nashar, Calixarene-doped PVC polymeric films as size-selective optical sensors: Monitoring of salicylate in real samples, *Spectrochim. Acta, Part A Mol. Biomol. Spectrosc.*, 2018, **201**, 98–104, DOI: 10.1016/J.SAA.2018.04.057.

15 F. M. Abdel-Haleem, Y. Alhashemi and M. S. Rizk, PVC membrane bulk optode incorporating 4-nitrobenzo-15-crown-5 and sodium tetrakis(1-imidazolyl) borate for the pico-molar determination of silver ion in pharmaceutical formulation, *Sci. Rep.*, 2024, **14**, 19984, DOI: 10.1038/S41598-024-70967-6.

16 E. Bakker, P. Bühlmann and E. Pretsch, Carrier-based ion-selective electrodes and bulk optodes. 1. General characteristics, *Chem. Rev.*, 1997, **97**, 3083–3132, DOI: 10.1021/cr940394a.

17 X. Du and X. Xie, Ion-Selective optodes: Alternative approaches for simplified fabrication and signaling, *Sens. Actuators, B Chem.*, 2021, **335**, 129368, DOI: 10.1016/J.SNB.2020.129368.

18 A. Barhoum, Y. Alhashemi, Y. M. Ahmed, M. S. Rizk, M. Bechelany and F. M. Abdel-haleem, *Innovations in Ion-Selective Optodes : a Comprehensive Exploration of Modern Designs and Nanomaterial Integration*, 2024, pp. 1–20, DOI: 10.3389/fbioe.2024.1397587.

19 K. J. Robinson, Y. Soda and E. Bakker, Recent improvements to the selectivity of extraction-based optical ion sensors, *Chem. Commun.*, 2022, **58**, 4279–4287, DOI: 10.1039/d1cc06636f.

20 P. Bühlmann, E. Pretsch and E. Bakker, Carrier-based ion-selective electrodes and bulk optodes. 2. Ionophores for potentiometric and optical sensors, *Chem. Rev.*, 1998, **98**(4), 1593–1688, DOI: 10.1021/cr970113+.

21 M. Lerchi, E. Bakker, B. Rusterholz and W. Simon, Lead-selective bulk optodes based on neutral ionophores with subnanomolar detection limits, *Anal. Chem.*, 2002, **64**, 1534–1540, DOI: 10.1021/AC00038A007.

22 N. V. Saranchina, Y. G. Slizhov, Y. M. Vodova, N. S. Murzakasymova, A. M. Ilyina, N. A. Gavrilenko and M. A. Gavrilenko, Smartphone-based colorimetric determination of fluoride anions using polymethacrylate optode, *Talanta*, 2021, **226**, 122103, DOI: 10.1016/J.TALANTA.2021.122103.

23 F. M. Abdel-Haleem, M. S. Rizk and M. M. El-Beshlawy, Molecularly-imprinted polymer-base bulk optode for the determination of ivabradine hydrochloride in Procoralan®, *RSC Adv.*, 2022, **12**, 17645–17654, DOI: 10.1039/D2RA02064E.
24 J. J. Belbruno, Molecularly Imprinted Polymers, *Chem. Rev.*, 2019, **119**(1), 94–119, DOI: 10.1021/acs.chemrev.8b00171.
25 G. Anantha-Iyengar, K. Shanmugasundaram, M. Nallal, K. P. Lee, M. J. Whitcombe, D. Lakshmi and G. Sai-Anand, Functionalized conjugated polymers for sensing and molecular imprinting applications, *Prog. Polym. Sci.*, 2019, **88**, 1–129, DOI: 10.1016/j.progpolymsci.2018.08.001.
26 J. Wang, R. Liang and W. Qin, Molecularly imprinted polymer-based potentiometric sensors, *TrAC, Trends Anal. Chem.*, 2020, **130**, 115980, DOI: 10.1016/j.trac.2020.115980.
27 A. Al Faysal, S. I. Kaya, A. Cetinkaya, S. A. Ozkan and A. Gölcü, The effect of polymerization techniques on the creation of molecularly imprinted polymer sensors and their application on pharmaceutical compounds, *Crit. Rev. Anal. Chem.*, 2025, **55**, 621–640.
28 F. M. Abdel-Haleem, A. Madbouly, R. M. El Nashar and N. T. Abdel-Ghani, Molecularly imprinted polymer-based bulk optode for the determination of itopride hydrochloride in physiological fluids, *Biosens. Bioelectron.*, 2016, **85**, 740–742, DOI: 10.1016/j.bios.2016.05.081.
29 Y. M. Ahmed, S. S. Badawy and F. M. Abdel-Haleem, Dibenzo-18-crown-6-based carbon paste sensors for the nanomolar potentiometric determination of daclatasvir dihydrochloride: An anti-HCV drug and a potential candidate for treatment of SARS-CoV-2, *Microchem. J.*, 2022, **177**, 107276, DOI: 10.1016/j.microc.2022.107276.
30 N. A. El Gohary, A. Madbouly, R. M. El Nashar and B. Mizaikoff, Synthesis and application of a molecularly imprinted polymer for the voltammetric determination of famciclovir, *Biosens. Bioelectron.*, 2015, **65**, 108–114, DOI: 10.1016/j.bios.2014.10.024.
31 N. T. Abdel Ghani, R. Mohamed El Nashar, F. M. Abdel-Haleem and A. Madbouly, Computational Design, Synthesis and Application of a New Selective Molecularly Imprinted Polymer for Electrochemical Detection, *Electroanalysis*, 2016, **28**, 1530, DOI: 10.1002/elan.201501130.
32 K. Y. Foo and B. H. Hameed, Insights into the modeling of adsorption isotherm systems, *Chem. Eng. J.*, 2010, **156**, DOI: 10.1016/j.cej.2009.09.013.
33 M. A. Fulazzaky, Understanding the adsorption isotherms and mass transfer kinetics for nonylphenol remediated by an adsorption method, *Next Research*, 2025, **2**, DOI: 10.1016/j.nexres.2025.100358.
34 J. Wang and X. Guo, Adsorption isotherm models: Classification, physical meaning, application and solving method, *Chemosphere*, 2020, **258**, DOI: 10.1016/j.chemosphere.2020.127279.
35 O. I. Parisi, M. Ruffo, L. Scrivano, R. Malivindi, A. Vassallo and F. Puoci, Smart Bandage Based on Molecularly Imprinted Polymers (MIPs) for Diclofenac Controlled Release, *Pharmaceuticals*, 2018, **11**, DOI: 10.3390/ph11040092.
36 E. Anticó, M. Lerchi, B. Rusterholz, N. Achermann, M. Badertscher, M. Valiente and E. Pretsch, Monitoring Pb2+ with optical sensing films, *Anal. Chim. Acta*, 1999, **388**, 327–338, DOI: 10.1016/S0003-2670(99)00085-9.
37 R. F. Alshehri, A. S. Amin and E. R. Darwish, Introducing an innovative immobilized optode based on PVC-ETH-5294 matrix for environmentally friendly sensing of lead ions, *Talanta Open*, 2024, **9**, 100285, DOI: 10.1016/J.TALO.2023.100285.
38 G. De Middeleer, P. Dubruel and S. De Saeger, Characterization of MIP and MIP functionalized surfaces: Current state-of-the-art, *TrAC Trends in Analytical Chemistry*, 2016, **76**, 71–85, DOI: 10.1016/j.trac.2015.11.007.
39 K. J. Devi, C. Shilpaja, K. Umasankar and K. Sushma, Development And In Vitro Assessment Of Melt In Mouth Tablets Of Lurasidone Hydrochloride, *J. Global Trends Pharm Sci*, 2017, **8**.
40 R. Shikalgar, V. Deshmukh, S. Rathod, G. S. Bangale, Y. V. Pore and D. P. Pawar, Fabrication of PF-127 Based Niosomal In Situ Gel for Intranasal Delivery of Lurasidone Hydrochloride and Optimization by Using 32 Factorial Design, *Bionanoscience*, 2024, **14**, 1318–1339, DOI: 10.1007/S12668-023-01290-Z.
41 M. M. El-Beshlawy, F. M. Abdel-Haleem and A. Barhoum, Molecularly Imprinted Potentiometric Sensor for Nanomolar Determination of Pioglitazone Hydrochloride in Pharmaceutical Formulations, *Electroanalysis*, 2021, **33**, 1244, DOI: 10.1002/elan.202060141.
42 K. Y. Goud, S. K. Kalisa, V. Kumar, Y. F. Tsang, S. E. Lee, K. V. Gobi and K. H. Kim, Progress on nanostructured electrochemical sensors and their recognition elements for detection of mycotoxins: A review, *Biosens. Bioelectron.*, 2018, **121**, 205–222, DOI: 10.1016/J.BIOS.2018.08.029.
43 P. Sharma, S. Sharma, B. Budhalakoti and H. Kumar, Thermodynamic characteristics and aggregation behavior of surface active ionic liquids in presence of vitamin B7 (biotin), *Tenside Surfactants Deterg.*, 2024, **61**, 345–357.
44 E. Bakker, M. Lerchi, T. Rosatzin, B. Rusterholz and W. Simon, Synthesis and characterization of neutral hydrogen ion-selective chromoionophores for use in bulk optodes, *Anal. Chim. Acta*, 1993, **278**, 211–225.
45 E. Wang and M. E. Meyerhoff, Anion selective optical sensing with metalloporphyrin-doped polymeric films, *Anal. Chim. Acta*, 1993, **283**, 673–682, DOI: 10.1016/0003-2670(93)85281-N.
46 Y. Qin and E. Bakker, Quantitive binding constants of H^+-selective chromoionophores and anion ionophores in solvent polymeric sensing membranes, *Talanta*, 2002, **58**, DOI: 10.1016/S0039-9140(02)00405-8.
47 S. M. Derayea, H. A. Elhamdy, K. M. Badr El-Din and M. Oraby, Versatile applications of a spectrofluorimetric approach based on photo-induced electron transfer blocking of Lurasidone, *J. Mol. Liq.*, 2023, **391**, 123264, DOI: 10.1016/j.molliq.2023.123264.